

Non-steady heating of cool cores of galaxy clusters by ubiquitous turbulence and AGN

Yutaka Fujita,^{1*} Renyue Cen,² and Irina Zhuravleva³

¹*Department of Earth and Space Science, Graduate School of Science, Osaka University, Toyonaka, Osaka 560-0043, Japan*

²*Department of Astrophysical Sciences, Princeton University, Princeton, NJ 08544, USA*

³*Department of Astronomy & Astrophysics, University of Chicago, Chicago, IL 60637, USA*

Accepted XXX. Received YYY; in original form ZZZ

ABSTRACT

Recent cosmological simulations have shown that turbulence should be generally prevailing in clusters because clusters are continuously growing through matter accretion. Using hydrodynamic simulations, we study the heating of cool-core clusters by the ubiquitous turbulence as well as feedback from the central active galactic nuclei (AGNs). We find that the AGN shows intermittent activities in the presence of moderate turbulence similar to the one observed with *Hitomi*. The cluster core maintains a quasi-equilibrium state for most of the time because the heating through turbulent diffusion is nearly balanced with radiative cooling. The balance is gradually lost because of slight dominance of the radiative cooling, and the AGN is ignited by increased gas inflow. Finally, when the AGN bursts, the core is heated almost instantaneously. Thanks to the pre-existing turbulence, the heated gas is distributed throughout the core without triggering thermal instability and causing catastrophic cooling, and the core recovers the quasi-equilibrium state. The AGN bursts can be stronger in lower-mass clusters. Predictions of our model can be easily checked with future X-ray missions like *XRISM* and *Athena*.

Key words: galaxies: clusters: general – galaxies: clusters: intracluster medium – galaxies: active – turbulence

1 INTRODUCTION

Radiative cooling time of the hot gas in intracluster medium (ICM) is often shorter than the Hubble time in the central regions of many galaxy clusters. In the absence of any heating sources, the hot gas in the core should cool and a flow toward the cluster centre should develop (a cooling flow; Fabian 1994). However, X-ray observations did not confirm the existence of massive cooling flows in clusters, suggesting that the cores are heated by some unknown sources (e.g. Ikebe et al. 1997; Peterson et al. 2001; Tamura et al. 2001; Kaastra et al. 2001). The most promising candidate of the heating source is active galactic nucleus (AGN) that resides in the cluster centre (e.g. Churazov et al. 2000; McNamara & Nulsen 2007; Fabian 2012). While there seems to be consensus that AGNs provide enough energy to counterbalance the radiative cooling, the question of how the energy is conveyed to the surrounding ICM is still under debate. So far, various mechanisms have been proposed, such as sound waves (Fabian et al. 2006, 2017; Zweibel et al. 2018), shocks (Randall et al. 2015;

Li et al. 2017), and cosmic-rays (Loewenstein et al. 1991; Guo & Oh 2008; Fujita & Ohira 2012; Fujita et al. 2013; Pfrommer 2013; Jacob & Pfrommer 2017; Ruszkowski et al. 2017; Su et al. 2019). If a cool core is assumed to be in a steady state, global stability needs to be considered. In fact, it is a serious problem for some heating models. For example, non-linear evolution of large-amplitude sound waves in clusters leads to localized heating, which destabilizes the core (Fujita & Suzuki 2005; Mathews et al. 2006).

Turbulence may be another carrier of heat in the ICM (Kim & Narayan 2003; Dennis & Chandran 2005; Ruszkowski & Oh 2010, 2011; Zhuravleva et al. 2014). Recently, *Hitomi* has discovered moderate turbulence in the Perseus cluster (Hitomi Collaboration et al. 2016). The ICM has a line-of-sight velocity dispersion of $164 \pm 10 \text{ km s}^{-1}$ in the region $r = 30\text{--}60$ kpc from the cluster centre. A similar level of turbulence in clusters has been measured from fluctuations of the X-ray surface brightness (Schuecker et al. 2004; Zhuravleva et al. 2014, 2018). Since *Hitomi* observed only a few small regions inside the core, it is unclear whether the

* E-mail: fujita@astro-osaka.jp

turbulence is created through the activities of the central AGN or not¹.

Here, we point out that AGNs are likely not the only source of turbulence in and around cluster cool cores. Cosmological numerical simulations have shown that the level of turbulence discovered by *Hitomi* can be explained by cluster formation (Lau et al. 2017; Ota et al. 2018). This reflects the fact that clusters are still growing, and gas and dark matter (as galaxies) are intermittently falling into them. This causes variations in cluster potential resulting in gas sloshing (Markevitch et al. 2001; Ascasibar & Markevitch 2006; ZuHone et al. 2019), and excites turbulence in the ICM (Fujita et al. 2004, 2005; ZuHone et al. 2013) even in apparently relaxed clusters (Lau et al. 2017; Ota et al. 2018). This ubiquitous turbulence is expected to convey thermal energy not only from the central AGN but also from the outside to the inside of a core. However, fairly strong turbulence (with the Mach number of $\gtrsim 0.3$ on scales $\gtrsim 100$ kpc; Zhuravleva et al. 2014) may be required to counterbalance the radiative cooling if AGN feedback is ignored.

In this study, we consider a heating model that incorporates the effects of simultaneous heating by both the central AGN and moderate turbulence excited by matter accretion onto clusters using 1D numerical simulations. We do *not* assume that a cool core is in a steady state. We focus on the global stability of the core and consider a wide range of parameters. Lau et al. (2017) and Bourne & Sijacki (2017) studied the simultaneous heating and indicated that large-scale bulk and shear motions associated with cluster growth can enhance the mixing and advection of AGN feedback energy. However, they investigated only limited cases. Our model is similar to a model that combines AGN feedback and thermal conduction (Ruszkowski & Begelman 2002). However, contrary to the latter, our model shows that a cluster core does not approach a steady state, and the central AGN intermittently bursts.

This paper is organized as follows. In Section 2, we describe our models on turbulence and AGN feedback. In Section 3, we show that the results of our numerical simulations. In Section 4, we discuss the implications of our results. Finally, Section 5 is devoted to conclusions. We assume a Λ CDM cosmology with $H_0 = 70 \text{ km s}^{-1} \text{ Mpc}^{-1}$ ($h = 0.7$), $\Omega_0 = 0.3$ and $\lambda = 0.7$.

2 MODELS

2.1 Hydrodynamic equations

We assume that clusters are spherically symmetric for the sake of simplicity. The flow equations are

$$\frac{\partial \rho}{\partial t} + \frac{1}{r^2} \frac{\partial}{\partial r} (r^2 \rho v) = \dot{\rho}_*, \quad (1)$$

$$\frac{\partial(\rho v)}{\partial t} + \frac{1}{r^2} \frac{\partial}{\partial r} (r^2 \rho v^2) = -\rho g - \frac{\partial P}{\partial r} - \dot{\rho}_* v, \quad (2)$$

¹ Recent results from optical observations indicated that turbulence at the centres of three clusters is driven by the AGNs (Li et al. 2019)

$$\begin{aligned} \frac{\partial e_g}{\partial t} + \frac{1}{r^2} \frac{\partial}{\partial r} (r^2 v e_g) &= -P \frac{1}{r^2} \frac{\partial}{\partial r} (r^2 v) + \frac{1}{r^2} \frac{\partial}{\partial r} \left(r^2 \kappa \frac{\partial T}{\partial r} \right) \\ &+ \frac{c_{\text{diss}} \rho u^3}{l} + \frac{1}{r^2} \frac{\partial}{\partial r} \left(r^2 D_{\text{eddy}} \rho T \frac{\partial s}{\partial r} \right) \\ &- n_e^2 \Lambda(T) + h_{\text{AGN}} - c_*, \end{aligned} \quad (3)$$

where t is the time, r is the cluster centric radius, ρ is the gas density, v is the bulk velocity, P is the pressure, T is the temperature, and s is the specific entropy. For other parameters, $\dot{\rho}_*$ is the mass-loss rate of stars per unit volume, u is the turbulent velocity, l is the dominant scale of turbulence, g is the gravitational acceleration, κ is the thermal conductivity, D_{eddy} is the eddy diffusivity, c_{diss} is a dimensionless constant, n_e is the electron number density, and Λ is the cooling function, h_{AGN} is the heating by the AGN, and c_* is the cooling due to mass-loss of stars in the brightest cluster galaxy (BCG) at the cluster centre. The energy density of gas is defined as $e_g = P/(\gamma - 1)$, where $\gamma = 5/3$. The second, third, and fourth terms of the right hand side of equation (3) represent thermal conduction, turbulent dissipation, and turbulent diffusion, respectively. The thermal conductivity is given by

$$\kappa(T) = 5 \times 10^{-7} f_c (T/\text{K})^{5/2} \quad (4)$$

in cgs units, where f_c is a reduction factor compared with the Spitzer value.

We assume that turbulence is induced through the growth of clusters and thus the turbulent velocity u should be related to the depth of the gravitational potential well. For simplicity, we assume that the AGN feedback does not affect the velocity u . Thus, we assume that

$$u(r) = \alpha_u V_{\text{cir}}(r), \quad (5)$$

where α_u is a parameter and V_{cir} is a circular velocity defined by the gravitational potential of the cluster (see equation [21]). For turbulent dissipation, we assume that $c_{\text{diss}} = 0.42$ (Dennis & Chandran 2005) and

$$l = \alpha_l r, \quad (6)$$

where α_l is an adjustable constant following Kim & Narayan (2003) and Dennis & Chandran (2005).

The eddy diffusivity is given by

$$D_{\text{eddy}} = c_{\text{td}} u l \xi, \quad (7)$$

where c_{td} is a dimensionless constant and ξ is a reduction factor. Following Dennis & Chandran (2005), we adopt $c_{\text{td}} = 0.11$ (see also Yeung 1994). The reduction factor is introduced considering the effects of buoyancy. If the dominant eddy-turnover frequency u/l is much smaller than the Brunt-Väisälä frequency,

$$N_{\text{BV}} = \sqrt{g \left(\frac{1}{\gamma P} \frac{dP}{dr} - \frac{1}{\rho} \frac{d\rho}{dr} \right)}, \quad (8)$$

then the radial motions are primarily determined by buoyancy oscillations with frequency N_{BV} . In this case, the radial displacement of a fluid element is $\sim u/N_{\text{BV}}$, which is much smaller than the eddy size l . Thus, the radial diffusion of heat is significantly suppressed by a factor of

$$\xi = \frac{1}{1 + c_0^2 l^2 N_{\text{BV}}^2 / u^2}, \quad (9)$$

where $c_0^2 = 0.1688$ (Weinstock 1981; Dennis & Chandran 2005).

For the cooling function, we adopt the following metallicity-dependent function:

$$\begin{aligned} \Lambda(T, Z) &= 2.41 \times 10^{-27} \left[0.8 + 0.1 \left(\frac{Z}{Z_\odot} \right) \right] \left(\frac{T}{\text{K}} \right)^{0.5} \\ &+ 1.39 \times 10^{-16} \left[0.02 + 0.1 \left(\frac{Z}{Z_\odot} \right)^{0.8} \right] \\ &\times \left(\frac{T}{\text{K}} \right)^{-1.0} \text{ erg cm}^3 \end{aligned} \quad (10)$$

(Fujita & Ohira 2013), which approximates the cooling function derived by Sutherland & Dopita (1993) for $T \gtrsim 10^5$ K and $Z \lesssim 1 Z_\odot$. Since we are interested in the central region of clusters, we adopt $Z = 0.5 Z_\odot$, hereafter.

2.2 Cluster potential

We assume that the potential of clusters is given by the NFW profile (Navarro et al. 1997). The density profile is given by

$$\rho_{\text{DM}}(r) = \frac{\delta_c \rho_c}{(r/r_s)(1+r/r_s)^2}, \quad (11)$$

where r_s is the characteristic radius, ρ_c is the critical density of the Universe, and δ_c is the normalization. We define the characteristic mass M_s as the mass enclosed within $r = r_s$. The halo concentration parameter is given by

$$c_\Delta = r_\Delta / r_s, \quad (12)$$

where r_Δ is the radius inside which the average density is Δ times the critical density of the Universe $\rho_c(z)$. From this definition, the mass inside r_Δ is given by

$$M_\Delta = \frac{4\pi}{3} \Delta \rho_c(z) r_\Delta^3. \quad (13)$$

The mass profile of the NFW profile is written as

$$M_{\text{NFW}}(r) = 4\pi \delta_c \rho_c r_s^3 \left[\ln \left(1 + \frac{r}{r_s} \right) - \frac{r}{r+r_s} \right]. \quad (14)$$

From this equation, the characteristic mass M_s can be expressed in terms of M_Δ and c_Δ :

$$M_s = M_\Delta \frac{\ln 2 - 1/2}{\ln(1+c_\Delta) - c_\Delta/(1+c_\Delta)}. \quad (15)$$

For a given M_Δ , the characteristic radius r_s , the mass M_s inside r_s , and the typical X-ray temperature in the inner region of the cluster T_c can be determined as follows. From the CLASH massive cluster sample (Postman et al. 2012), Fujita et al. (2018a) found that the cluster X-ray temperature T_c has a tight correlation with r_s and M_s :

$$T_c = T_{c0} \left(\frac{r_s}{r_{s0}} \right)^{-2} \left(\frac{M_s}{M_{s0}} \right)^{3/2}, \quad (16)$$

where (r_{s0}, M_{s0}, T_{c0}) is a representative point of the relation (Fujita et al. 2018b).² Note that T_c is the temperature at

$r = 50\text{--}500$ kpc from the cluster centre. For $\Delta = 200$, the concentration parameter is represented by

$$c_{200}(M_{200}, z) = 6.71 \left(\frac{M_{200}}{2 \times 10^{12} h^{-1} M_\odot} \right)^{-0.091} (1+z)^{-0.44} \quad (17)$$

for $M_{200} \sim 10^{11}\text{--}10^{15} h^{-1} M_\odot$ and $z < 2$ (Duffy et al. 2008; see also Bhattacharya et al. 2013; Dutton & Macciò 2014; Meneghetti et al. 2014; Diemer & Kravtsov 2015; Correa et al. 2015). This relation has a large dispersion, which makes a variety of T_c for a given mass (Fujita et al. 2018b) but we ignore it here. For a given z and M_{200} , r_s and M_s can be derived from equations (12), (15) and (17), and thus T_c is obtained from equation (16). We assume $z = 0$, hereafter.

We also include the stellar contribution of the brightest cluster galaxy (BCG) to the gravitational acceleration. For the Perseus cluster ($M_{200} \sim 8.5 \times 10^{14} M_\odot$; Mathews et al. 2006), it is

$$g_{*0}(r) = \left[\left(\frac{r^{0.5975}}{3.206 \times 10^{-7}} \right)^{9/10} + \left(\frac{r^{1.849}}{1.861 \times 10^{-6}} \right)^{9/10} \right]^{-10/9} \text{ cm s}^{-2}, \quad (18)$$

where r is in kpc (Mathews et al. 2006). Since the mass of a BCG is weakly correlated to the mass of the host halo ($M_{\text{BCG}} \propto M_{200}^{0.4}$; Kravtsov et al. 2018; Erfanianfar et al. 2019), we scale the acceleration as $g_* = g_{*0}(M_{200}/8.5 \times 10^{14} M_\odot)^{0.4}$. Thus, the total acceleration is

$$g(r) = g_*(r) + \frac{GM_{\text{NFW}}(r)}{r^2}, \quad (19)$$

where G is the gravitational constant. The stellar mass profile of the BCG is written as

$$M_*(r) = g_*(r) r^2 / G. \quad (20)$$

The circular velocity of the cluster is given by

$$V_{\text{cir}}(r) = \sqrt{\frac{GM(r)}{r}} = \sqrt{g(r)r}. \quad (21)$$

where $M(r) = M_*(r) + M_{\text{NFW}}(r)$ is the total mass profile. The velocity profile is time-independent.

2.3 AGN heating

We adopt a simple model for AGN heating. We assume that the total heating rate depends on the mass accretion rate $\dot{M} = -4\pi r^2 \rho v$ ($v < 0$) at the inner boundary of the simulation region ($r = r_{\text{in}}$).

The Eddington accretion rate is given by

$$\dot{M}_{\text{Edd}} = L_{\text{Edd}} / c^2, \quad (22)$$

where $L_{\text{Edd}} = 1.3 \times 10^{38} (M_{\text{BH}}/M_\odot) \text{ erg s}^{-1}$ is the Eddington luminosity and M_{BH} is the black hole mass³. We assume that the black hole mass is proportional to the stellar mass of the BCG. Since the mass of the black hole at the centre of the Perseus cluster is $1 \times 10^9 M_\odot$ (Nagai et al. 2019), we assume

³ The Eddington accretion rate is defined as $\dot{M}_{\text{Edd}} = 10 L_{\text{Edd}}/c^2$ in Yuan & Narayan (2014). For this definition, an advection-dominated accretion flow is realized at $\dot{M}/\dot{M}_{\text{Edd}} \lesssim 0.01$.

² We use $r_{s0} = 414$ kpc, $M_{s0} = 1.4 \times 10^{14} M_\odot$, and $T_{c0} = 3.7$ keV based on the results of the MUSIC simulations (Meneghetti et al. 2014; Fujita et al. 2018a).

that $M_{\text{BH}} = 1 \times 10^9 M_{\odot} (M_{200}/8.5 \times 10^{14} M_{\odot})^{0.4}$. The total heating rate is given by

$$L_{\text{AGN}} = \epsilon \eta(\dot{M}) \dot{M} c^2, \quad (23)$$

where $\epsilon < 1$ is the heating efficiency and $\eta(\dot{M})$ is a correction factor. We introduce ϵ because not all of the rest-mass energy of the gas engulfed by the black hole is used to heat the ICM. Moreover, not all the gas that passed the inner boundary (r_{in}) reaches the black hole; some of it will form stars in the BCG. The correction factor reflects the fact that the nature of an accretion flow changes at $\dot{M}/\dot{M}_{\text{Edd}} \sim 0.1$ (Yuan & Narayan 2014). In particular, an advection-dominated accretion flow that is realized at $\dot{M}/\dot{M}_{\text{Edd}} \lesssim 0.1$ has a low radiative efficiency. Thus, we assume that $\eta = 1$ for $\dot{M}/\dot{M}_{\text{Edd}} > 0.1$ and

$$\eta = \frac{\dot{M}}{0.1 \dot{M}_{\text{Edd}}} \quad (24)$$

for $\dot{M}/\dot{M}_{\text{Edd}} < 0.1$ following Yuan & Narayan (2014).

The heating rate per the unit volume is given by

$$h_{\text{AGN}}(r) = \frac{L_{\text{AGN}}}{4\pi(r_{\text{AGN}} - r_{\text{in}})r^2}, \quad (25)$$

where r_{AGN} is the maximum radius inside which the AGN heating is effective. For $r > r_{\text{AGN}}$, we assume $h_{\text{AGN}}(r) = 0$. The radial dependence of $h_{\text{AGN}} \propto r^{-2}$ may be realized if the ICM is heated at the surface of some kind of waves or fronts of which surface area increases as $\propto r^2$. The radius of the heated region is assumed to be $r_{\text{AGN}} = 50$ kpc, based on the fact that the central AGN disturbs the ambient ICM on a scale of ~ 50 kpc for the Perseus cluster (Sanders & Fabian 2007). Note that if the heating rate is represented by $h_{\text{AGN}} \propto r^{-\beta}$, β and r_{AGN} are degenerated. If $\beta (> 0)$ is larger and/or r_{AGN} is smaller, the heating is more centrally concentrated. We find that if the heating is too much concentrated (e.g. $\beta = 2$ and $r_{\text{AGN}} = 20$ kpc), the mixing of hot and cool gas is not enough and thermal instability develops.

2.4 Stellar mass-loss

The gas ejected from stars in the BCG mixes with the surrounding ICM. This serves as cooling in equation (3), because the mass-loss gas is cooler than the ambient ICM. This gas may be the cause of multi-temperature structure of the ICM around the cluster centre.

The cooling rate due to the mass-loss gas is given by

$$c_* = -\alpha_* \rho_* \left(\epsilon_0 - \frac{P}{\rho} - \epsilon_{\text{ICM}} + \frac{1}{2} v^2 \right), \quad (26)$$

where $\epsilon_{\text{ICM}} = 3kT/(2\mu m_p)$ is the specific thermal energy of the ICM, k is the Boltzmann constant, and $\mu = 0.61$ is the mean molecular weight (Mathews & Brighenti 2003). The specific mass loss-rate is $\alpha_* = 4.7 \times 10^{-20} \text{ s}^{-1}$ at $z \sim 0$ (Mathews & Brighenti 2003). The stellar mass density $\rho_*(r)$ can be derived from equation (20) and the mass-loss rate is written as $\dot{\rho}_* = \alpha_* \rho_*$ in equation (2). The source term $\alpha_* \rho_* (\epsilon_0 - P/\rho - \epsilon_{\text{ICM}})$ represents the heating of the hot ICM of specific energy ϵ_{ICM} by the mean energy of stellar ejecta ϵ_0 less the work done P/ρ in displacing the hot gas. The term $\alpha_* \rho_* v^2/2$ represents dissipative heating. The mean gas injection energy is $\epsilon_0 = 3kT_0/(2\mu m_p)$, where $T_0 = (\alpha_* T_* + \alpha_{\text{sn}} T_{\text{sn}})/\alpha_*$. The stellar temperature mainly reflects the

Table 1. Model parameters

Model	M_{200} ($10^{14} M_{\odot}$)	α_u	α_l	variation	ϵ	f_c
M35	8.5	0.3	0.5	no	0.01	0
M25	8.5	0.2	0.5	no	0.01	0
M55	8.5	0.5	0.5	no	0.01	0
M33	8.5	0.3	0.3	no	0.01	0
M35v	8.5	0.3	0.5	yes	0.01	0
M35e	8.5	0.3	0.5	no	0.1	0
M25c	8.5	0.2	0.5	no	0.01	0.2
L35/L35b	5.5	0.3	0.5	no	0.01	0
H35	14	0.3	0.5	no	0.01	0

kinetic energy of stars and is given by $T_* = (\mu m_p/k)\sigma_*^2$, where σ_* is the stellar velocity dispersion of the BCG. Here, we assume a typical value of $\sigma_* = 275 \text{ km s}^{-1}$ (Loubser et al. 2009) and the following results are not sensitive to the value. The characteristic temperature of supernovae is written as $T_{\text{sn}} = 2\mu m_p E_{\text{sn}}/(3kM_{\text{sn}})$, where $E_{\text{sn}} = 10^{51} \text{ erg}$ is the explosion energy of a supernova and M_{sn} is the ejecta mass. The specific mass loss rate from supernovae is $\alpha_{\text{sn}} \approx 2 \times 10^{-22} (M_{\text{sn}}/M_{\odot}) \text{ s}^{-1}$ at $z \sim 0$, in which the mass-to-light ratio is assumed to be ~ 10 (Mathews & Brighenti 2003). The product $\alpha_{\text{sn}} T_{\text{sn}}$ does not depend on M_{sn} and α_{sn} is much smaller than α_* .

3 RESULTS

The hydrodynamic equations (1)-(3) are solved by a second-order advection upstream splitting method (AUSM) based on Liou & Steffen (1993; see also Wada & Norman 2001). We set the inner and outer boundary at $r_{\text{min}} = 3$ and $r_{\text{max}} = 500$ kpc, respectively. We use 300 unequally spaced meshes in the radial coordinate to cover the region. The innermost mesh has a width of ~ 40 pc, and the width of the outermost mesh is ~ 10 kpc. The following boundary conditions are adopted. (1) Variables except velocity have zero gradients at the centre. (2) The inner edge is assumed to be a perfectly reflecting point. (3) The density and pressure at the outermost mesh are equal to specified initial values. Initially, the ICM is in a hydrostatic equilibrium and isothermal at $T = T_c$. We solve the hydrodynamic equations with turbulence and thermal conduction off until temperature at the inner boundary drops to $T = 2$ keV in order to create a cool core quickly. Then, we turn on turbulence and thermal conduction, and set this time for $t = 0$. We calculate until $t = 8$ Gyr, which is the look-back time of $z \sim 1$.

3.1 Fiducial model

Table 1 shows our models and parameters. As a fiducial model (M35), we choose turbulence parameters as $\alpha_u = 0.3$ (equation [5]) and $\alpha_l = 0.5$ (equation [6]). The cluster mass is $M_{200} = 8.5 \times 10^{14} M_{\odot}$, which gives $c_{200} = 4.0$ and $T_c = 4.6$ keV (section 2.2). The accretion efficiency for the AGN heating is $\epsilon = 0.01$ (equation [23]) and thermal conduction is ignored ($f_c = 0$; equation [4]).

Figure 1 shows the radial profile of the 1D turbulent velocity $u_{1D} \equiv u/\sqrt{3}$ given by equation (5). The velocity

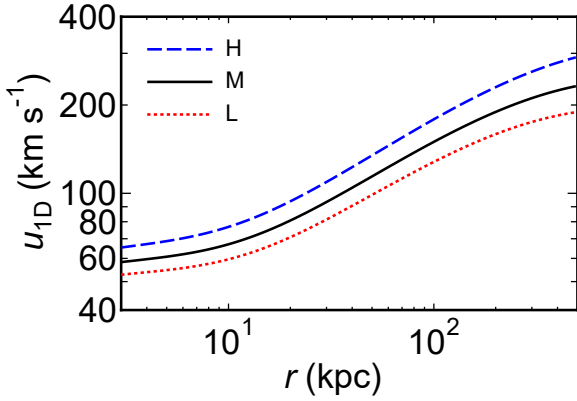


Figure 1. Profiles for the 1D turbulent velocity when $\alpha_u = 0.3$. Blue dashed, solid black, and dotted red lines show the cases of $M_{200} = 1.4 \times 10^{15}$, 8.5×10^{14} , and $5.5 \times 10^{14} M_\odot$, respectively.

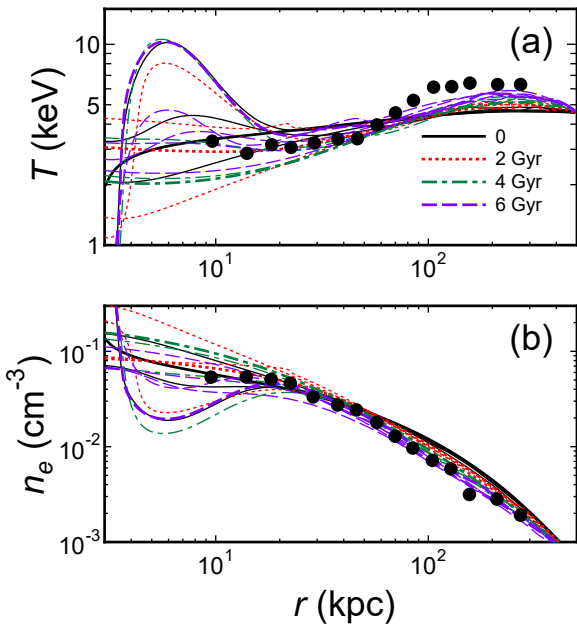


Figure 2. (a) Temperature and (b) electron density profiles for model M35. Thick lines correspond to specific times; solid black line gives $t = 0$, dotted red line gives $t = 2$ Gyr, dash-dotted green line gives $t = 4$ Gyr, and dashed purple line gives $t = 6$ Gyr. Thin lines show the profiles at 0.5 Gyr intervals; solid black lines give $t = 0.5$ –1.5 Gyr, dotted red lines give $t = 2.5$ –3.5 Gyr, dash-dotted green lines give $t = 4.5$ –5.5 Gyr, and dashed purple lines give $t = 6.5$ –8 Gyr. Black dots are observations of the Perseus cluster (Zhuravleva et al. 2015). Errors are omitted because vertical ones are small compared with the dot size.

is $u_{1D} \sim 110 \text{ km s}^{-1}$ at $r \sim 50 \text{ kpc}$, which is comparable to the value derived from the latest analysis of the *Hitomi* data for the Perseus cluster (Hitomi Collaboration et al. 2018). The velocity gradually increases outward as is predicted by cosmological numerical simulations (e.g. Ota et al. 2018). *Hitomi* observations have also shown that the spatial scale of turbulence is $< 100 \text{ kpc}$ for $r \lesssim 100 \text{ kpc}$ (Hitomi Collaboration et al. 2018). Thus, our choice of $\alpha_l = 0.5$ is consistent with the result. Our assumption is also consistent with the amplitude of motions estimated from density

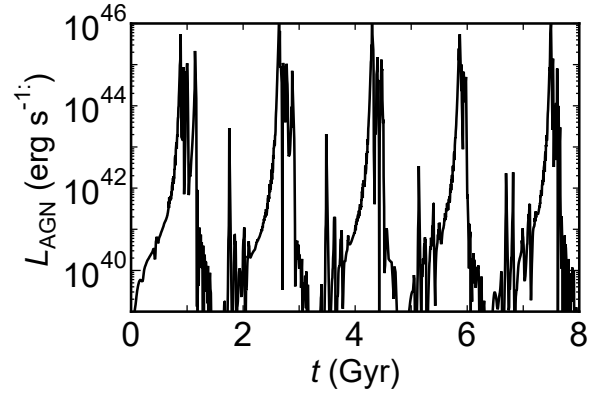


Figure 3. Variation of AGN power for model M35.

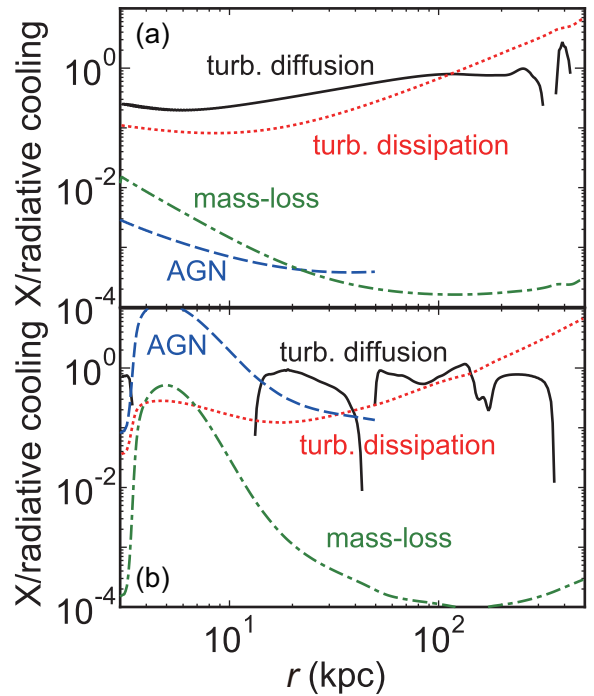


Figure 4. Ratios of heating and stellar mass-loss terms (X) to the radiative cooling term ($n_e^2 \Lambda(T)$) on the right hand side of equation (3) at (a) $t = 4$ Gyr and (b) $t = 1$ Gyr for model M35. Dashed red line: turbulent dissipation (third term). Solid black line: turbulent diffusion (fourth term). Dashed blue line: AGN heating (h_{AGN}). Dash-dotted green line: stellar mass-loss (c_*). Turbulent diffusion term is not shown when it is negative.

fluctuations in the central regions of ten clusters (~ 100 – 300 km s^{-1} on scales of $\lesssim 100 \text{ kpc}$; Zhuravleva et al. 2018).

Figure 2 shows the profiles of temperature and density at various times. The temperature and density at $r \lesssim 10 \text{ kpc}$ fluctuate wildly owing to the changing AGN activities shown in Figure 3. In Figure 2, we plotted observational data for the Perseus cluster (Zhuravleva et al. 2015) as a reference. Although we do not fine-tune the cluster parameters (e.g. c_{200}), our results broadly reproduce the observations. Figure 2 indicates that the temperature sometimes reaches $\sim 10 \text{ keV}$ at $r \lesssim 10 \text{ kpc}$ at strong bursts of the AGN ($t \sim 1.0, 2.6, 4.3, 5.9,$ and 7.5 Gyr in Figure 3). During the bursts, the cool core will be significantly disturbed, although 3D simulations

are required to discuss actual morphology. Turbulent diffusion gradually smooths out the hot region without causing catastrophic instabilities and distributes the energy injected by the bursts across the core. This process is similar to a previous mixing model (Hillel & Soker 2016, 2017). In their model, however, gas is mixed through gas motion generated by AGN activities contrary to our model where turbulent mixing is driven by structure formation. We note that our 1D results shown in Figure 2 implicitly assume that gas is well-mixed in the tangential direction and could not directly be compared with observations for the innermost region of clusters ($\lesssim 10$ kpc), where multi-temperature structures and bubbles have been observed. In that region, hot tenuous gas and cool dense gas often coexist at the same radius (e.g. Sanders et al. 2004), and the azimuthally averaged temperature and density are observationally biased toward the cool dense gas. The temperature of the inside of the bubbles may be much larger than 10 keV (Abdulla et al. 2019).

The periodical activities of the AGN shown in Figure 3 indicate that radiative cooling is not balanced with the AGN heating at a given time. The excessive cooling increases \dot{M} and L_{AGN} (equation [23]). Figure 4a shows the ratios of heating terms to the radiative cooling term $n_e^2 \Lambda(T)$ in equation (3) at $t = 4$ Gyr when the AGN activity is not strong (Figure 3). The turbulent diffusion term is the most important heating source for $r \lesssim 100$ kpc and the turbulent dissipation term comes next. Contributions of the AGN and stellar mass-loss are negligible. If the two turbulence terms are combined, the ratio to the radiative cooling becomes close to one but still smaller than unity. This means that the cluster core is in a quasi-equilibrium state. However, since the turbulent heating (dissipation plus diffusion) does not fully counterbalance the radiative cooling, the cooling gradually overwhelms the heating and the mass inflow rate \dot{M} increases. This finally leads to strong AGN bursts. Figure 4b shows the ratios at $t = 1$ Gyr when the AGN is active (Figure 3). The AGN heating exceeds radiative cooling at $r \lesssim 10$ kpc.

In Figure 4, turbulent dissipation surpasses turbulent diffusion at $r \gtrsim 100$ kpc. This leads to gradual increase of temperature in that region (Figure 2). In a real cluster this can be attributed to the increase of mass and temperature of the cluster because the turbulence is induced by matter accretion from the outside of the cluster. It is well known that when a cluster forms, the kinetic energy associated with the bulk motion of infalling gas is converted to thermal energy at shocks. The turbulent heating is another process of the energy conversion. We expect that the turbulent energy dissipation rate is related to the mass accretion rate of the cluster.

3.2 Dependence on turbulence parameters

Figure 5 shows the temperature and density profiles for model M25. This model gives weaker turbulence ($\alpha_u = 0.2$) than the fiducial model M35 ($\alpha_u = 0.3$). Since the turbulent diffusion is insufficient, the temperature and density in the central region fluctuate with a larger amplitude than those for model M35, and hot and cool gas are not well mixed. As a result, the temperature around the centre reaches zero at $t = 2.2$ Gyr, which prevents us from further calculation. This shows that a certain level of turbulence is required for

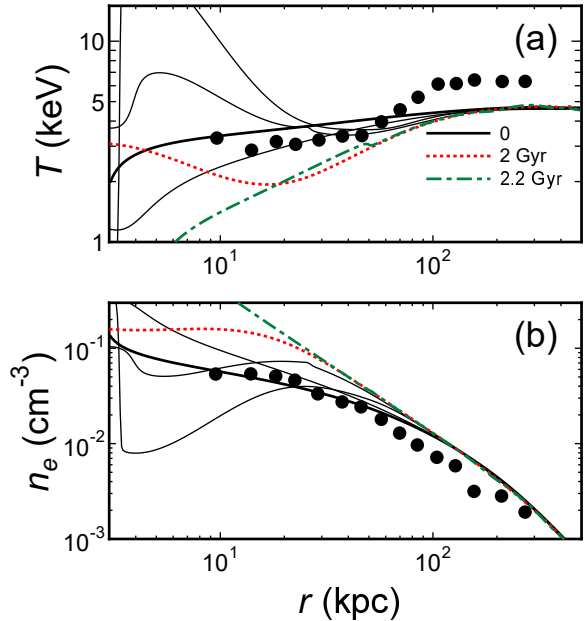


Figure 5. Same as Figure 2 but for model M25. Dash-dotted line shows $t = 2.2$ Gyr or the end of calculation.

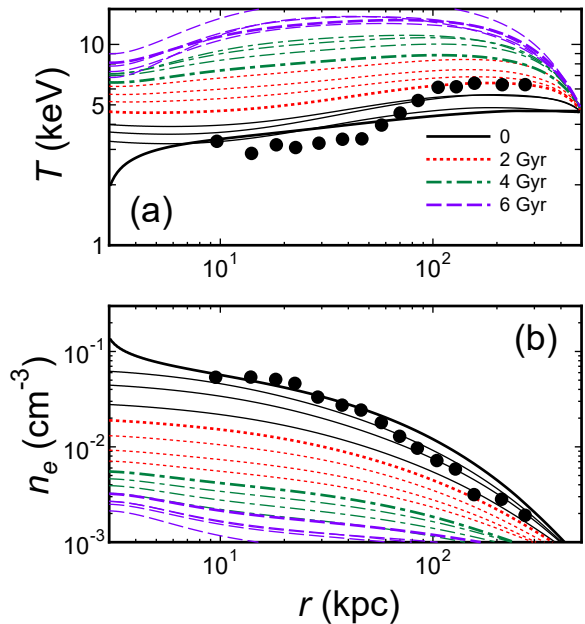


Figure 6. Same as Figure 2 but for model M55.

smooth heating to be consistent with the temperature floor of observed clusters.

The temperature and density profiles for model M55 ($\alpha_u = 0.5$) are presented in Figure 6. Since the turbulent heating dominates radiative cooling, the temperature significantly increases while the density decreases. Although clusters are growing and their temperature increases, the rapid evolution in Figure 6 seems to be inconsistent with actual clusters (e.g. Eke et al. 1998). Thus, it may be unrealistic that clusters constantly have turbulence as strong as that in model M55. The appropriate level of turbulence should be discussed in the context of cluster mass accretion rate.

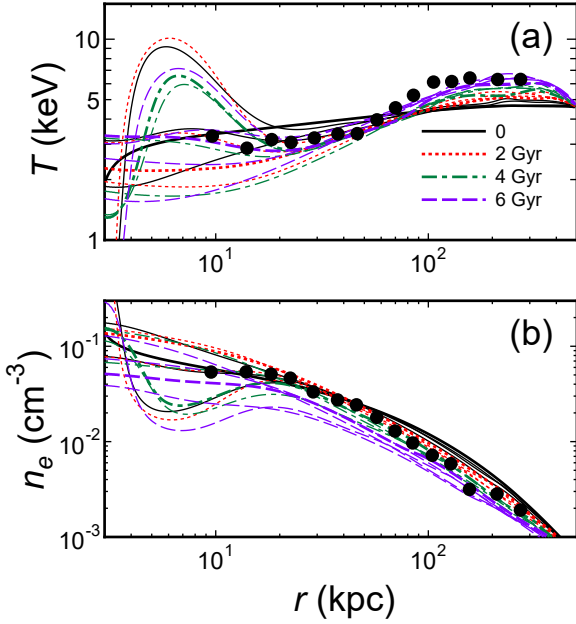


Figure 7. Same as Figure 2 but for model M33.

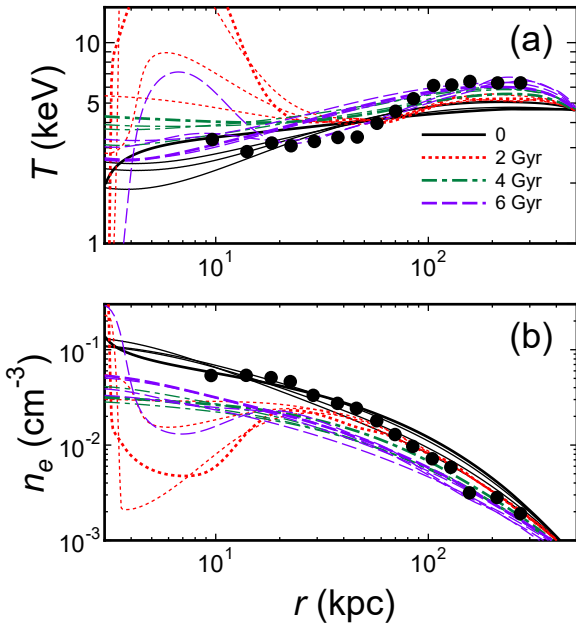


Figure 8. Same as Figure 2 but for model M35v.

Figure 7 shows the results of model M33 ($\alpha_l = 0.3$) in which the size of eddies is smaller than that in the fiducial model M35 ($\alpha_l = 0.5$). The results of the two models are similar (Figures 7 and 2). Thus, turbulent heating is not sensitive to the eddy size compared with the velocity of the turbulence (α_u).

In real clusters, turbulence in the ICM is expected to vary. For example, it is likely that turbulence is intensified during cluster mergers. In order to study the effects of time-variation, we study model M35v in which turbulent velocity is given by

$$u(r) = \alpha_u(1 + 0.5 \cos(t/t_p))V_{\text{cir}}(r), \quad (27)$$

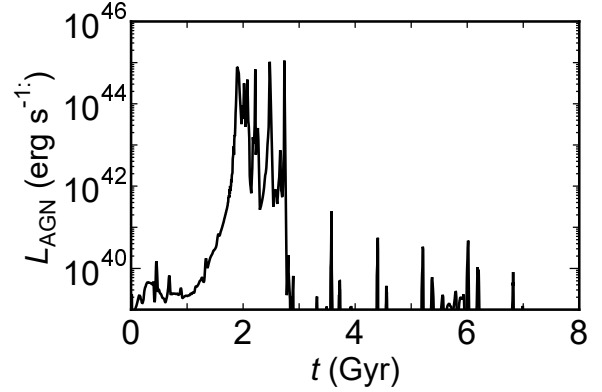


Figure 9. Same as Figure 3 but for model M35v.

where $t_p = 0.5$ Gyr; other parameters are the same as model M35. Figures 8 and 9 show that the cluster is affected by strong AGN bursts at $t \sim 2$ Gyr. The central ICM is heated and the cool core is almost destroyed by the bursts. Then, the ICM slowly cools through radiative cooling and the cool core is reshaped. The AGN does not burst strongly during this period. These results suggest that AGN activities are not necessarily periodic in real clusters as opposed to model M35 (Figure 3).

3.3 AGN efficiency and thermal conduction

Figures 10–12 show the results for model M35e, in which the accretion efficiency ($\epsilon = 0.1$) is larger than the fiducial model M35 ($\epsilon = 0.01$). The efficiency $\epsilon = 0.1$ is probably the maximum value in the sense that all inflow gas is swallowed by the black hole and all the energy generated by the AGN with an efficiency of 10% goes to the ICM. The temperature and density profiles are similar between the two models (Figures 10 and 2). While the AGN shows periodic bursts in both models (Figures 11 and 3), the activity is less spiky in model M35e. In Figure 12a, we show the energy balance during a burst phase. The AGN generates energy large enough to counterpart the radiative cooling with less accretion rate. Thus, the response to radiative cooling and the subsequent increase of the mass accretion rate becomes milder. During a quiet phase, the contribution of the AGN is minor (Figure 12b). We have also studied the evolution when $\epsilon = 0.001$. In this case, we find that the AGN activity is too spiky to be smoothed out by turbulence.

Figures 13–15 show the results for model M25c. In this model, thermal conduction of $f_c = 0.2$ (see equation [3]) is included. The value of f_c is expected when magnetic fields are chaotic (Narayan & Medvedev 2001). In model M25 ($f_c = 0$), hot and cool gas is not well mixed and the calculations stop at 2.2 Gyr (Figure 5). In model M25c, on the contrary, thermal conduction assists the mixture and the calculation completes a period of 8 Gyr (Figures 13 and 14), although the fluctuations of temperature and density in the central region are larger (Figure 13). Figure 15 shows the balance between heating and cooling at $t = 4$ Gyr; thermal conduction significantly contributes as a heating source at $r \sim 80$ kpc.

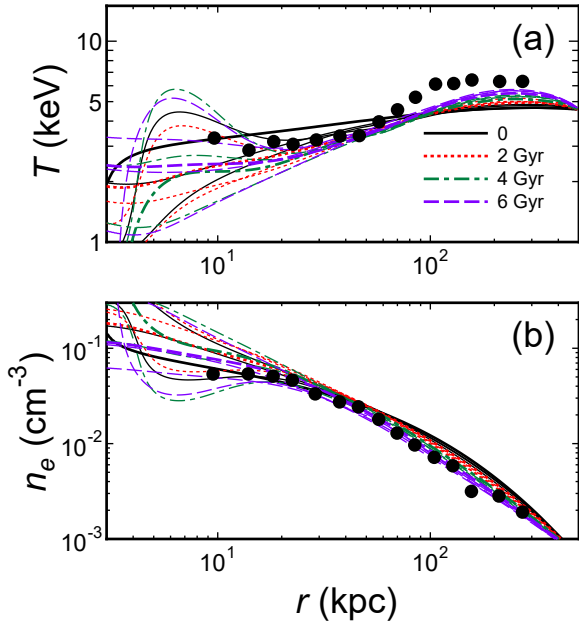


Figure 10. Same as Figure 2 but for model M35e.

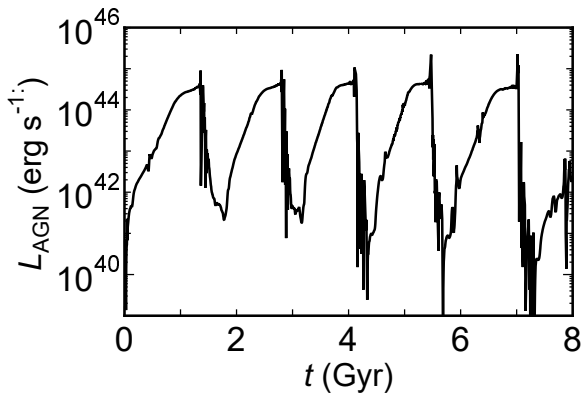
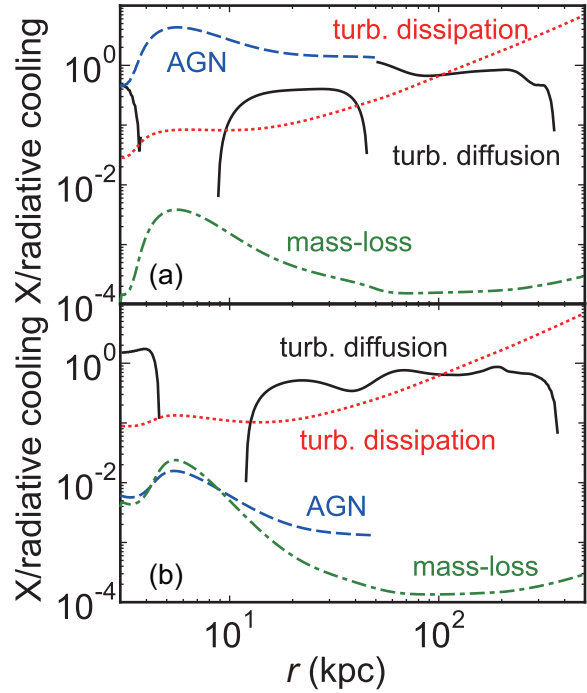


Figure 11. Same as Figure 3 but for model M35e.

3.4 Dependence on cluster mass

In Figure 16, we present the results for model L35, in which the cluster mass ($M_{200} = 5.5 \times 10^{14} M_{\odot}$) is smaller than that in model M35 ($M_{200} = 8.5 \times 10^{14} M_{\odot}$). This mass gives $c_{200} = 4.2$ and $T_c = 3.3$ keV (section 2.2). As a reference, we show the observational results for Hydra A cluster (David et al. 2001), which has a temperature close to T_c . The turbulent velocity profile we assumed is shown in the dotted red line in Figure 1. The evolution is similar to the fiducial model (model M35; Figures 2). However, this result depends on our assumption that the AGN heating is less powerful in less massive clusters ($M_{\text{BCG}} \propto M_{200}^{0.4}$ and $M_{\text{BH}} \propto M_{\text{BCG}}$). Observations have shown that the $M_{\text{BCG}}-M_{200}$ relation has a large scatter (Kravtsov et al. 2018; Erfanianfar et al. 2019), and some less massive clusters have a fairly massive BCG. In order to study this case, we consider a model in which M_{BCG} and M_{BH} are the same as model M35, while other parameters are the same as model L35. We call this model L35b and show the results in Figure 17. Compared with Figure 16, the fluctuations of temperature and density are larger, which reflects

Figure 12. Same as Figure 4 but for model M35e at (a) $t = 4$ Gyr and (b) $t = 3$ Gyr.

stronger AGN bursts. If the strong AGN activities are associated with jets launched by the AGN, large-scale shocks may be created due to their kinetic power. These shocks may be the ones observed in some less massive clusters (e.g. MS0735.6+7421, Hercules A, and Hydra A; McNamara et al. 2005; Nulsen et al. 2005a,b; Simionescu et al. 2009).

Figure 18 shows the results for model H35 with $M_{200} = 1.4 \times 10^{15} M_{\odot}$ ($c_{200} = 3.8$ and $T_c = 6.8$ keV). We show the observational results for the Abell 2029 cluster as a reference (Paterno-Mahler et al. 2013). In this model, the influence of the AGN bursts is less significant, because the contribution of the AGN heating is less prominent ($M_{\text{BH}}/M_{200} \propto M_{200}^{-0.6}$) and the turbulent velocity is larger (Figure 1).

4 DISCUSSION

Since clusters of galaxies are still growing, we expect that a certain level of turbulence always exists in the ICM. We have considered AGN feedback in the cool core of a cluster when moderate turbulence prevails in the core. The results of our numerical simulations show that the AGN activity is intermittent with occasional bursts. During the quiet phase in general, radiative cooling of the cool core is nearly balanced with the heating through turbulent diffusion and turbulence dissipation (sum of both), and the AGN contribution to the heating is minor. Turbulent diffusion conveys thermal energy from the outside of the core. However, when the turbulent velocity is moderate ($\alpha_u \sim 0.3$), the turbulent heating (diffusion plus dissipation) cannot completely offset the radiative cooling, although it can prolong the quiet period and reduce the frequency of the AGN bursts. Similar bursty behaviours of the AGN have been studied for elliptical galaxies (Ciotti & Ostriker 2007; Ciotti et al. 2017). Contrary to the

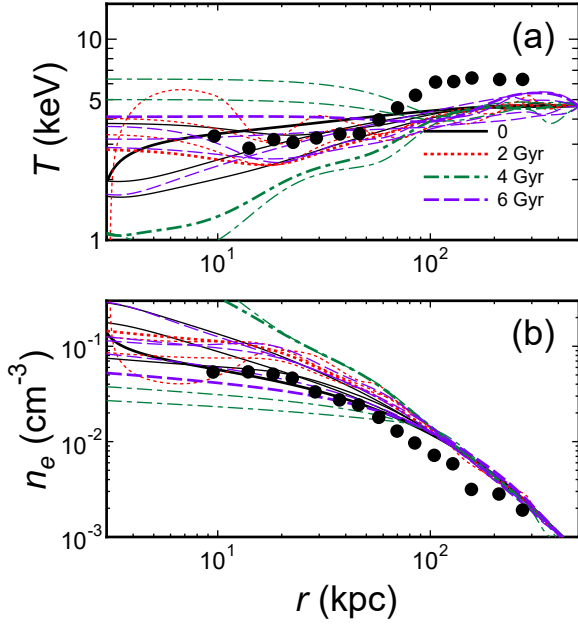


Figure 13. Same as Figure 2 but for model M25c.

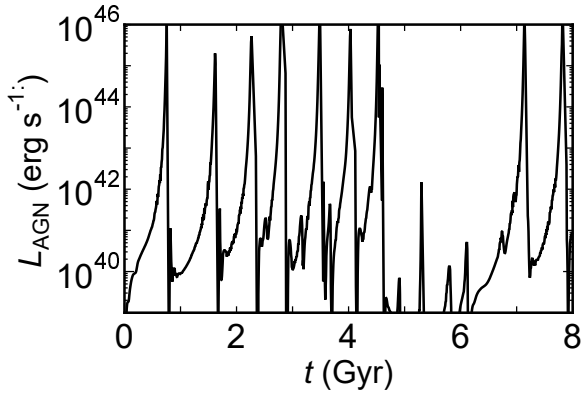


Figure 14. Same as Figure 3 but for model M25c.

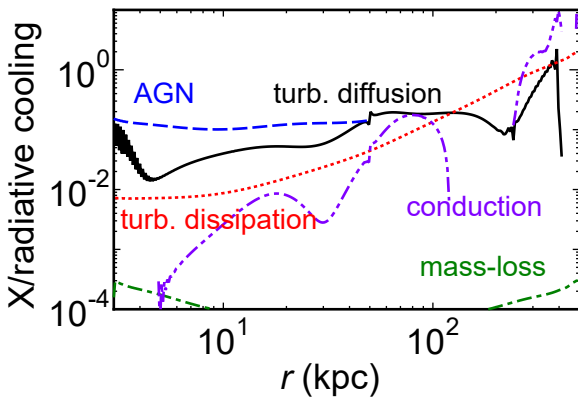


Figure 15. Same as Figure 4 but for model M25c at $t = 4$ Gyr. Two-dotted-dashed purple line shows thermal conduction (second term on the right hand side of equation [3])

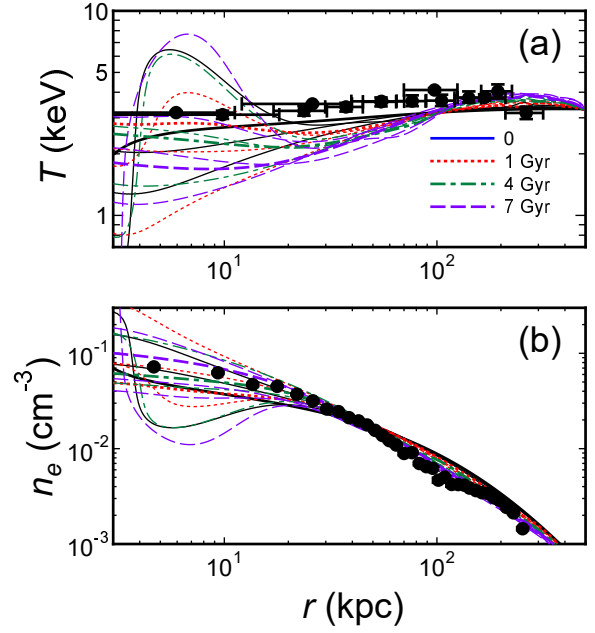


Figure 16. Same as Figure 2 but for model L35. Black dots are observations for the Hydra A cluster (David et al. 2001).

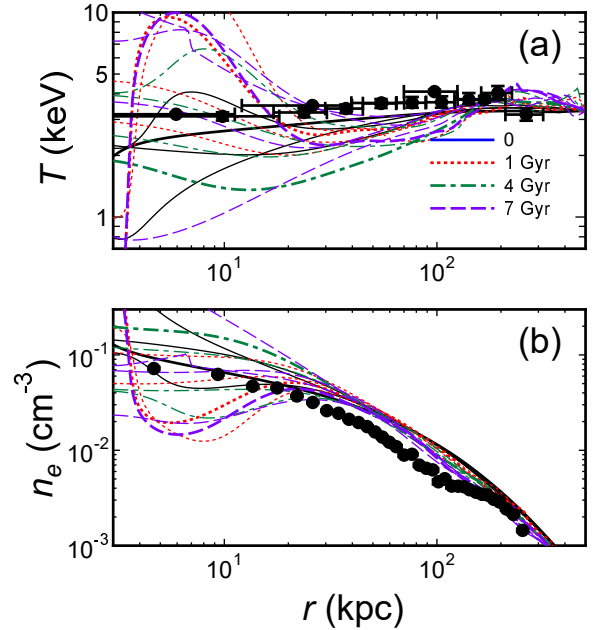


Figure 17. Same as Figure 16 but for model L35b.

case of an isolated elliptical galaxy, the BCG at the centre of a cool core is affected by external factors such as an inflow from the outside and turbulence induced by cluster growth. These effects influence the frequency and duration of the AGN bursts as we have shown in this study.

Our model of AGN heating is very simple (section 2.3), and our results suggest that even such an “unsophisticated” model works. That is, subtle balance between the AGN heating and radiative cooling is not required, because turbulence smoothes out strong temperature and density inhomogeneity and a cool core does not need to be in a

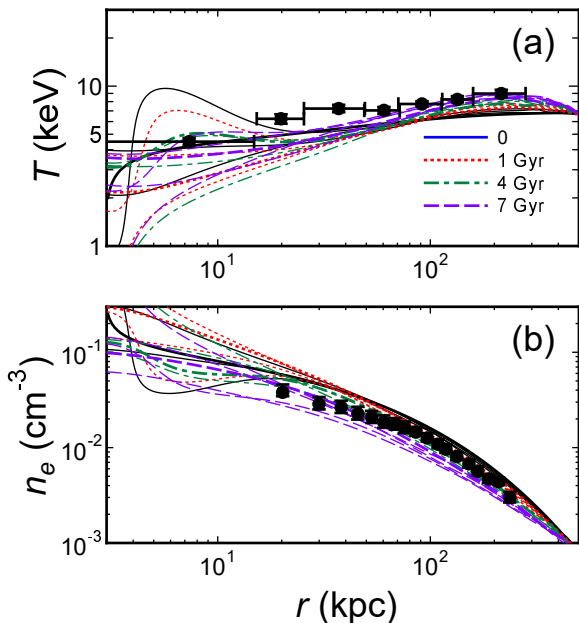


Figure 18. Same as Figure 2 but for model H35. Black dots are observations for the Abell 2029 cluster (north direction) (Paterno-Mahler et al. 2013).

steady state. Unless the heating is not too centrally concentrated, a wide variety of heating models would be allowed. In the vicinity of the AGN ($r \ll 1$ kpc), which cannot be resolved in our simulations, thermal instabilities may develop and stimulate AGN activities (McCourt et al. 2012; Sharma et al. 2012; Barai et al. 2012; Gaspari et al. 2013; Guo & Mathews 2014; Meece et al. 2015). While these activities may increase the AGN heating rate, they can be regarded as local phenomena as long as their contribution is minor compared to the turbulent heating. Thus, we do not expect tight correlations between AGN properties and global properties of the host cluster.

Our simulations show that the velocity of turbulence must be in a certain range ($\alpha_u \sim 0.3$) in order to avoid violent heating and/or cooling (section 3.2). If the velocity is too small, turbulence cannot sufficiently mix hot and cool gas, which leads to catastrophic cooling (Figure 5). If it is too large, the cluster is strongly heated through turbulent dissipation and the cluster temperature rises too rapidly (Figure 6). This indicates that clusters cannot sustain turbulence with such a large α_u for a long time considering an actual mass accretion rate and history of the clusters. However, α_u may temporally be boosted by a cluster merger. In this case, the cool core would be destroyed and the cluster turns into a non-cool core cluster (even though our formulation is developed for cool-core clusters).

The level of turbulence in clusters will be predicted more precisely by cosmological numerical simulations with a high resolution. Previous studies showed that the ratio of turbulent pressure to total pressure in the central region of clusters is typically an order of $\sim 10\%$, although there is a considerable variation among clusters (e.g. Nelson et al. 2014; Vazza et al. 2018). The value is roughly consistent with our assumption. Observationally, the level will be measured with high-spectral resolution X-ray missions such as *X-ray Imag-*

*ing and Spectroscopy Mission (XRISM)*⁴ and *Athena*⁵ in the future. In particular, it could be checked whether that turbulent regions have a flat entropy profile or they correspond to high-entropy regions that are radially connected to each other if turbulence actually transports heated gas around the AGN and/or outside the core. Since there could be strong azimuthal variation, mapping observations of turbulence are essential. Moreover, AGN activities in clusters with strong turbulence (generated through cluster growth) tend to be weak. This could also be observed in the future X-ray missions.

We note that the value of $\alpha_u \sim 0.3$ may change in more realistic 3D simulations that reproduce complicated gas motions in clusters. Also our simulations do not explicitly include turbulence created by the central AGN. If the contribution is significant, the turbulence created through cluster growth does not need to be as strong as we assumed. In order to study the turbulence driven by an AGN, X-ray observations of turbulence around the AGN will be useful. Moreover, more realistic models of AGN feedback that include generation of turbulence, bubbles and shocks should be considered. The heating by AGN jets in turbulent ICM has been studied with 3D numerical simulations (Lau et al. 2017; Bourne & Sijacki 2017). Although they investigated the feedback under restricted circumstances, they showed that the pre-existing turbulence associated with cluster growth can enhance the mixing and advection of AGN feedback energy, which is consistent with our results. On the other hand, if observations prove that actual turbulence in clusters is generally not enough to sustain stable heating, it may mean that thermal conduction is working in cluster cores (section 3.3).

In our model, less massive clusters can show violent AGN activities if the ratio between the BCG mass and the host cluster mass is large (section 3.4). This means that the cool cores of those clusters tend to be destroyed. This tendency may be confirmed with *eROSITA* by observing many clusters and measuring their M_{BCG}/M_{200} with various methods, while the destruction of cool cores by cluster mergers also needs to be taken into account. Moreover, large-scale shocks created through past strong AGN bursts (e.g. MS0735.6+7421; McNamara et al. 2005) would commonly be observed in those clusters. The ratio M_{BCG}/M_{200} may be larger at high redshifts because galaxies form earlier than clusters in a standard hierarchical clustering scenario. Thus, a larger fraction of cool cores may be destroyed by AGN activities.

5 CONCLUSIONS

We have studied a new class of time-dependent cool core models in which radiative cooling is offset by a combination of central AGN heating and moderate turbulence excited through cluster growth. We found that a cool core does not achieve a steady state and the AGN shows intermittent activities. The core is in a quasi-equilibrium state for most of the time because the heating through turbulent diffusion

⁴ <http://xrism.isas.jaxa.jp/en/>

⁵ <https://www.the-athena-x-ray-observatory.eu/>

(dominant) and dissipation are nearly balanced with radiative cooling. The contribution of the AGN heating is minor during this phase. The balance between cooling and heating is eventually lost because of slight dominance of the cooling. The mass accretion rate toward the central black hole increases and finally the AGN bursts. As a result, the core is almost instantaneously heated. Since the already-existing turbulence mixes the heated gas with surrounding gas, the core does not suffer catastrophic cooling through thermal instability and recovers the quasi-equilibrium state. The AGN bursts can be stronger in lower-temperature clusters if the ratio of the BCG mass to the cluster mass is large. Future X-ray missions such as *XRISM* and *Athena* will be able to test our predictions.

Our study is based on 1D simulation and our model of AGN feedback is rather simple. For more quantitative discussion, 3D cosmological simulations and more realistic AGN feedback models would be desirable.

ACKNOWLEDGEMENTS

This work was supported by MEXT KAKENHI Nos. 18K03647 (Y.F.).

REFERENCES

- Abdulla Z., et al., 2019, *ApJ*, **871**, 195
 Ascasibar Y., Markevitch M., 2006, *ApJ*, **650**, 102
 Barai P., Proga D., Nagamine K., 2012, *MNRAS*, **424**, 728
 Bhattacharya S., Habib S., Heitmann K., Vikhlinin A., 2013, *ApJ*, **766**, 32
 Bourne M. A., Sijacki D., 2017, *MNRAS*, **472**, 4707
 Churazov E., Forman W., Jones C., Böhringer H., 2000, *A&A*, **356**, 788
 Ciotti L., Ostriker J. P., 2007, *ApJ*, **665**, 1038
 Ciotti L., Pellegrini S., Negri A., Ostriker J. P., 2017, *ApJ*, **835**, 15
 Correa C. A., Wyithe J. S. B., Schaye J., Duffy A. R., 2015, *MNRAS*, **452**, 1217
 David L. P., Nulsen P. E. J., McNamara B. R., Forman W., Jones C., Ponman T., Robertson B., Wise M., 2001, *ApJ*, **557**, 546
 Dennis T. J., Chandran B. D. G., 2005, *ApJ*, **622**, 205
 Diemer B., Kravtsov A. V., 2015, *ApJ*, **799**, 108
 Duffy A. R., Schaye J., Kay S. T., Dalla Vecchia C., 2008, *MNRAS*, **390**, L64
 Dutton A. A., Macciò A. V., 2014, *MNRAS*, **441**, 3359
 Eke V. R., Navarro J. F., Frenk C. S., 1998, *ApJ*, **503**, 569
 Erfanianfar G., et al., 2019, arXiv e-prints, p. arXiv:1908.01559
 Fabian A. C., 1994, *ARA&A*, **32**, 277
 Fabian A. C., 2012, *ARA&A*, **50**, 455
 Fabian A. C., Sanders J. S., Taylor G. B., Allen S. W., Crawford C. S., Johnstone R. M., Iwasawa K., 2006, *MNRAS*, **366**, 417
 Fabian A. C., Walker S. A., Russell H. R., Pinto C., Sanders J. S., Reynolds C. S., 2017, *MNRAS*, **464**, L1
 Fujita Y., Ohira Y., 2012, *ApJ*, **746**, 53
 Fujita Y., Ohira Y., 2013, *MNRAS*, **428**, 599
 Fujita Y., Suzuki T. K., 2005, *ApJ*, **630**, L1
 Fujita Y., Matsumoto T., Wada K., 2004, *ApJ*, **612**, L9
 Fujita Y., Matsumoto T., Wada K., Furusho T., 2005, *ApJ*, **619**, L139
 Fujita Y., Kimura S., Ohira Y., 2013, *MNRAS*, **432**, 1434
 Fujita Y., Umetsu K., Rasia E., Meneghetti M., Donahue M., Medezinski E., Okabe N., Postman M., 2018a, *ApJ*, **857**, 118
 Fujita Y., Umetsu K., Ettori S., Rasia E., Okabe N., Meneghetti M., 2018b, *ApJ*, **863**, 37
 Gaspari M., Ruszkowski M., Oh S. P., 2013, *MNRAS*, **432**, 3401
 Guo F., Mathews W. G., 2014, *ApJ*, **780**, 126
 Guo F., Oh S. P., 2008, *MNRAS*, **384**, 251
 Hillel S., Soker N., 2016, *MNRAS*, **455**, 2139
 Hillel S., Soker N., 2017, *MNRAS*, **466**, L39
 Hitomi Collaboration et al., 2016, *Nature*, **535**, 117
 Hitomi Collaboration et al., 2018, *PASJ*, **70**, 9
 Ikebe Y., et al., 1997, *ApJ*, **481**, 660
 Jacob S., Pfrommer C., 2017, *MNRAS*, **467**, 1449
 Kaastra J. S., Ferrigno C., Tamura T., Paerels F. B. S., Peterson J. R., Mittaz J. P. D., 2001, *A&A*, **365**, L99
 Kim W.-T., Narayan R., 2003, *ApJ*, **596**, L139
 Kravtsov A. V., Vikhlinin A. A., Meshcheryakov A. V., 2018, *Astronomy Letters*, **44**, 8
 Lau E. T., Gaspari M., Nagai D., Coppi P., 2017, *ApJ*, **849**, 54
 Li Y., Ruszkowski M., Bryan G. L., 2017, *ApJ*, **847**, 106
 Li Y., et al., 2019, arXiv e-prints, p. arXiv:1911.06329
 Liou M.-S., Steffen C. J., 1993, *Journal of Computational Physics*, **107**, 23
 Loewenstein M., Zweibel E. G., Begelman M. C., 1991, *ApJ*, **377**, 392
 Loubser S. I., Sánchez-Blázquez P., Sansom A. E., Soechting I. K., 2009, *MNRAS*, **398**, 133
 Markevitch M., Vikhlinin A., Mazzotta P., 2001, *ApJ*, **562**, L153
 Mathews W. G., Brighenti F., 2003, *ARA&A*, **41**, 191
 Mathews W. G., Faltenbacher A., Brighenti F., 2006, *ApJ*, **638**, 659
 McCourt M., Sharma P., Quataert E., Parrish I. J., 2012, *MNRAS*, **419**, 3319
 McNamara B. R., Nulsen P. E. J., 2007, *ARA&A*, **45**, 117
 McNamara B. R., Nulsen P. E. J., Wise M. W., Rafferty D. A., Carilli C., Sarazin C. L., Blanton E. L., 2005, *Nature*, **433**, 45
 Meece G. R., O'Shea B. W., Voit G. M., 2015, *ApJ*, **808**, 43
 Meneghetti M., et al., 2014, *ApJ*, **797**, 34
 Nagai H., et al., 2019, *ApJ*, **883**, 193
 Narayan R., Medvedev M. V., 2001, *ApJ*, **562**, L129
 Navarro J. F., Frenk C. S., White S. D. M., 1997, *ApJ*, **490**, 493
 Nelson K., Lau E. T., Nagai D., 2014, *ApJ*, **792**, 25
 Nulsen P. E. J., Hambrick D. C., McNamara B. R., Rafferty D., Birzan L., Wise M. W., David L. P., 2005a, *ApJ*, **625**, L9
 Nulsen P. E. J., McNamara B. R., Wise M. W., David L. P., 2005b, *ApJ*, **628**, 629
 Ota N., Nagai D., Lau E. T., 2018, *PASJ*, **70**, 51
 Paterno-Mahler R., Blanton E. L., Randall S. W., Clarke T. E., 2013, *ApJ*, **773**, 114
 Peterson J. R., et al., 2001, *A&A*, **365**, L104
 Pfrommer C., 2013, *ApJ*, **779**, 10
 Postman M., et al., 2012, *ApJS*, **199**, 25
 Randall S. W., et al., 2015, *ApJ*, **805**, 112
 Ruszkowski M., Begelman M. C., 2002, *ApJ*, **581**, 223
 Ruszkowski M., Oh S. P., 2010, *ApJ*, **713**, 1332
 Ruszkowski M., Oh S. P., 2011, *MNRAS*, **414**, 1493
 Ruszkowski M., Yang H. Y. K., Reynolds C. S., 2017, *ApJ*, **844**, 13
 Sanders J. S., Fabian A. C., 2007, *MNRAS*, **381**, 1381
 Sanders J. S., Fabian A. C., Allen S. W., Schmidt R. W., 2004, *MNRAS*, **349**, 952
 Schuecker P., Finoguenov A., Miniati F., Böhringer H., Briel U. G., 2004, *A&A*, **426**, 387
 Sharma P., McCourt M., Quataert E., Parrish I. J., 2012, *MNRAS*, **420**, 3174
 Simionescu A., Roediger E., Nulsen P. E. J., Brüggén M., Forman W. R., Böhringer H., Werner N., Finoguenov A., 2009, *A&A*, **495**, 721
 Su K.-Y., et al., 2019, *MNRAS*, p. 2649
 Sutherland R. S., Dopita M. A., 1993, *ApJS*, **88**, 253
 Tamura T., et al., 2001, *A&A*, **365**, L87
 Vazza F., Angelinelli M., Jones T. W., Eckert D., Brüggén M., Brunetti G., Gheller C., 2018, *MNRAS*, **481**, L120

- Wada K., Norman C. A., 2001, [ApJ](#), **547**, 172
Weinstock J., 1981, [J. Geophys. Res.](#), **86**, 9925
Yeung P. K., 1994, [Physics of Fluids](#), **6**, 3416
Yuan F., Narayan R., 2014, [ARA&A](#), **52**, 529
Zhuravleva I., et al., 2014, [Nature](#), **515**, 85
Zhuravleva I., et al., 2015, [MNRAS](#), **450**, 4184
Zhuravleva I., Allen S. W., Mantz A., Werner N., 2018, [ApJ](#), **865**, 53
ZuHone J. A., Markevitch M., Brunetti G., Giacintucci S., 2013, [ApJ](#), **762**, 78
ZuHone J. A., Zavala J., Vogelsberger M., 2019, [ApJ](#), **882**, 119
Zweibel E. G., Mirnov V. V., Ruszkowski M., Reynolds C. S., Yang H. Y. K., Fabian A. C., 2018, [ApJ](#), **858**, 5

This paper has been typeset from a $\text{\TeX}/\text{\LaTeX}$ file prepared by the author.